

Automatic image-based respiratory signal extraction in real-time CMR

Chong Chen,¹ Yingmin Liu,² Orlando P. Simonetti,^{2,4,5} Rizwan Ahmad^{1,2,3}

1 Biomedical Engineering, The Ohio State University, Columbus OH, USA

2 Davis Heart & Lung Research Institute, The Ohio State University, Columbus OH, USA

3 Electrical and Computer Engineering, The Ohio State University, Columbus OH, USA

4 Internal Medicine, The Ohio State University, Columbus OH, USA

5 Radiology, The Ohio State University, Columbus OH, USA

* Corresponding author:

Name Chong Chen

Department Biomedical Engineering

Institute The Ohio State University

Address 460 W 12th Ave, Room 311
Columbus OH 43210, USA

E-mail chen.7211@osu.edu

Manuscript word count: 4,086

Abstract word count: 190

Abstract

Purpose: To develop a fully automatic method for extraction and directionality determination of respiratory signal in free-breathing, real-time (RT) cardiac MRI.

Methods: The respiratory signal is extracted by a principal component analysis method from RT cine images. Then, a two-step procedure is used to determine the directionality (sign) of the respiratory signal. First, the signal polarity of all slices is made consistent with a reference slice. Second, a global sign correction is performed by maximizing the correlation of the respiratory signal with the zeroth-moment center curve. The proposed method is evaluated in multi-slice RT cine from eleven volunteers and two patients. The motion in a manually selected region-of-interest is used as reference.

Results: The extracted respiratory signal using the proposed method exhibits high, positive correlation with the reference in all cases and is more robust compared to a recently proposed method. To demonstrate its clinical utility, the method is used to identify heartbeats from inspiratory and expiratory phases and, in turn, to account for respiration-induced changes in the cardiac output.

Conclusions: The proposed method enables fully automatic extraction and directionality determinations of respiratory signal from RT cardiac cine images, allowing accurate cardiac function quantification.

Keywords: directionality determination, respiratory motion, principal component analysis, real-time cardiac cine, MRI

INTRODUCTION

Cardiovascular magnetic resonance imaging (CMR) is the gold standard to evaluate cardiac morphology and ventricular function. To reduce the influence of respiratory and cardiac motion, breath-held (BH) segmented k-space acquisitions are widely used in CMR. However, such protocols can be challenging for patients with poor respiratory control or arrhythmia. Moreover, they are unable to capture the influence of respiratory motion on the cardiac output. As a result, there is a growing demand to develop real-time (RT) CMR methods that are insensitive to arrhythmia and respiratory motion. In RT cardiac cine, 2D slices are collected sequentially under free-breathing conditions. Recently proposed advanced data acquisition and image reconstruction methods have allowed the spatial and temporal resolution of RT cine to rival that of the traditional BH segmented acquisition (1, 2, 3). After image reconstruction, one complete heartbeat from each slice can be used for cardiac function quantification. To get accurate and reproducible cardiac function measurements, all selected heartbeats must belong to a single respiratory phase, e.g., peak-expiration (4, 5). Right ventricular quantification, in particular, has been shown to be sensitive to the respiratory phase (6).

Navigator echoes are commonly used for prospective compensation of respiratory motion (7). Such techniques, however, do not allow imaging across the entire cardiac cycle and are not compatible with steady-state free-precession sequences, which are commonly used for cardiac cine. External devices, such as belts or pillow bellows with pressure sensors, are also able to measure the respiratory signal (8). However, these devices require prior setup, must be synchronized with the MRI acquisition, and do not work reliably in patients. Consequently, they are not commonly used in clinical practice. Self-gating has also been proposed for RT imaging, where the same k-space location is sampled repeatedly during the scan (9). The resulting signal is then processed to extract cardiac and respiratory signals. For Cartesian sampling, however, this strategy requires modifying the pulse sequence and can lower the overall efficiency to accommodate the increased repetition time or the additional self-gating readouts (10). Alternatively, the respiratory signal can be extracted directly from reconstructed RT images collected without sacrificing acquisition efficiency. In the MRI literature, several image-based strategies for respiratory signal extraction have been reported. For example, methods based on tracking lung air density, diaphragm motion, image center of mass, and image registration have been proposed (11, 12, 13, 14). However, in these methods, the image features with pronounced respiratory motion must be selected manually. Also, such features may not be consistently visible in all slices.

Instead of tracking image features, several recently proposed methods rely on principal component analysis (PCA) for respiratory motion extraction. PCA-based methods map the high-dimensional image series to a low dimensional space, while preserving salient spatiotemporal information. Such methods have been successfully used to extract the respiratory signal from PET, CT, and MRI images (15, 16, 17). Extensions of PCA, such as kernel-PCA and Laplacian eigenmaps, have also been employed for respiratory signal extraction (18, 19, 20, 21). A major challenge for such methods is that the extracted signal has an uncertain directionality (i.e., arbitrary sign) with respect to the physical motion, which means that the maximal signal could refer to either inspiration or expiration. An inconsistent directionality assignment to respiratory signals from different slices in the cine stack can lead to a mixing of heartbeats from inspiration and expiration phases, which can impact cardiac function quantification. A simple approach to correctly assign directionality is to assume that more time is spent in expiration than inspiration (19). However, this assumption does not hold consistently across all subjects and is only applicable when there are several respiratory cycles available. To resolve this issue, more robust methods have been proposed. For example, Bertolli et al. (22) resolved the directionality ambiguity in PET images by assuming the directionality of the respiration-induced cranio-caudal motion of the internal organs. For MRI, Novillo et al. (17) recently proposed an unsupervised directionality determination method based on tracking the diaphragmatic motion or estimating the lung volume, but this method requires selecting the lung-diaphragm interface on cine image series.

This study is an extension of our preliminary work (23), where a fully automatic method to extract directionality-resolved respiratory signal from a stack of RT cardiac cine was proposed and evaluated in healthy volunteers. In this work, we further optimize the algorithm, include additional data from patients, and make a direct comparison to the recently proposed method by Novillo et al. (17), which is referred to as Unsupervised Respiratory signal Extraction (URE). Also, to demonstrate clinical utility, we use the proposed method to segregate peak-expiration and peak-inspiration heartbeats from each slice and show the respiratory motion-induced variations in cardiac output in volunteers.

THEORY

Extraction of the respiratory signal

An overview of the extraction of the respiratory signal is given in Fig. 1. Consider an image series with N frames and M pixels per frame. First, we filter the images using a low pass filter $[0 - 0.8 \text{ Hz}]$ along the temporal dimension to suppress the higher frequency components, e.g., from the cardiac motion. After vectorizing each frame, the image series from the j^{th} slice can be represented by matrix, $\mathbf{D}_j \in \mathbb{R}^{M \times N}$, with each column corresponding to a single frame. Then, we subtract the temporal mean from \mathbf{D}_j and construct the covariance matrix $\mathbf{\Sigma}_j \in \mathbb{R}^{N \times N}$ using Eqs. 1 and 2, i.e.,

$$\tilde{\mathbf{D}}_j(m, n) = \mathbf{D}_j(m, n) - \frac{1}{N} \sum_{n'=1}^N \mathbf{D}_j(m, n') \quad [1]$$

$$\mathbf{\Sigma}_j = \tilde{\mathbf{D}}_j^T \tilde{\mathbf{D}}_j \quad [2]$$

The eigen decomposition of $\mathbf{\Sigma}_j$ is performed to obtain right singular vectors, $\{\vec{v}_{j,1}, \vec{v}_{j,2}, \dots, \vec{v}_{j,N}\}$, of $\tilde{\mathbf{D}}_j$. These singular vectors capture different motions present in $\tilde{\mathbf{D}}_j$, including the respiratory motion. Since the cardiac motion has been suppressed via low-pass filtering, the first singular vector, $\vec{v}_{j,1}$, is expected to represent the respiratory signal. Lastly, the 1st ‘‘eigen image’’ from the j^{th} slice is obtained by $\mathbf{D}_j \vec{v}_{j,1}$, which can be interpreted as a projection of the image series on the corresponding respiratory signal, $\vec{v}_{j,1}$, and is used in the directionality determination procedure described below. For brevity, we drop the second subscript and represent the extracted respiratory motion in the j^{th} slice by \vec{v}_j .

Directionality determination

As Illustrated in Fig. 2, we adopt a two-step procedure to resolve directionality (sign) ambiguity in the respiratory motion from multi-slice RT cardiac cine. In the first step, we choose the 1st slice ($j = 1$) as reference and adjust the signs of all the other slices ($j = 2, 3, \dots, J$) with respect to the reference. To this end, we estimate Pearson correlation coefficient, $r_{j,j+1}$, between $\mathbf{D}_j \vec{v}_j$ and $\mathbf{D}_{j+1} \vec{v}_{j+1}$ and adjust the sign of \vec{v}_{j+1} based on

$$\vec{v}_{j+1} = \text{sign}\left(\prod_{l=1}^{l=j} r_{l,l+1}\right) \vec{v}_{j+1} \quad [3]$$

where \vec{v}_{j+1} represents sign-corrected singular vector from the $(j+1)^{\text{th}}$ slice. For the example shown in Fig. 2(a), the correlation between the eigen images from the 1st and 2nd slices, $r_{1,2}$, is negative, which results in sign flipping of \vec{v}_2 (i.e., $\vec{v}_2 = -\vec{v}_2$) to make it consistent with the reference \vec{v}_1 . For the 3rd slice, in contrast, the sign is not flipped (i.e., $\vec{v}_3 = \vec{v}_3$) since $\prod_{l=1}^{l=2} r_{l,l+1} = r_{1,2}r_{2,3}$ is positive, which indicates that the 3rd slice is already consistent with the reference. This process is repeated for all values of j as depicted in Fig. 2(a). Note, only the pair-wise correlations between two adjacent slices are used for adjusting the sign. The eigen images from non-adjacent slices may not be strongly correlated due to dissimilar image content. As a result, adjusting the sign of $j > 2$ slices based on their correlation with $j = 1$ slice is not expected to be reliable. Upon the conclusion of this step, the sign of \vec{v}_j is consistent across slices but is still arbitrary with respect to the directionality of the respiratory motion and thus cannot distinguish inspiration from expiration.

In the second step, we use the temporal profile of the zeroth-moment center (ZMC) of the image intensity to perform the overall sign correction. The movement of the thoracic and abdominal organs as a function of respiration is predictable in the superior-inferior (SI) direction (24). In particular, ZMC is expected to move superiorly with expiration and inferiorly with inspiration and thus can be used to guide the sign correction. Let $\vec{c}_j \in \mathbb{R}^{N \times 1}$ represent ZMC across N frames from the j^{th} slice. To compute \vec{c}_j , we first identify the image axis that has a larger component in the SI direction. The information regarding the precise orientation of the imaging plane is readily available in the Digital Imaging and Communications in Medicine (DICOM) file header. Using this information, we reorient the image such that the vertical axis has the larger component in the SI direction and the top-to-bottom direction of the reoriented image is aligned with superior-to-inferior direction of the subject. Then, we construct the SI projection $\mathbf{P}_j \in \mathbb{R}^{L \times N}$ of the image series $\mathbf{I}_j \in \mathbb{R}^{R \times L \times N}$ by summing the R pixels along the horizontal direction, where L is the number of pixels in the vertical axis. For the m^{th} pixel in the i^{th} frame (column) of \mathbf{P}_j , its distance from ZMC is defined as: $d(m, i, j) = \sum_{l=1}^m \mathbf{P}_j(l, i) - \sum_{l=1}^L \mathbf{P}_j(l, i)/2$. We find $m^* \geq \text{ZMC}$ that minimizes this displacement, i.e.,

$$m^* = \operatorname{argmin}_m d(m, i, j) \quad \text{s.t.} \quad d(m, i, j) \geq 0, \quad m \in \{1, 2, \dots, L\}. \quad [4]$$

Finally, the ZMC for the i^{th} frame and j^{th} slice is obtained by:

$$\vec{c}_j(i) = m^* - \frac{d(m^*, i, j)}{d(m^*, i, j) - d(m^* - 1, i, j)}, \quad [5]$$

where $d(m^*, i, j) \geq 0$, $d(m^* - 1, i, j) < 0$, and $\vec{c}_j(i) \in (m^* - 1, m^*]$ is the linearly interpolated zero crossing of $d(m, i, j)$.

The collective sign of \vec{v}_j is adjusted by

$$\vec{v}_j = \text{sign} \left[\sum_{j'=1}^J \text{sign}(s_{j'}) \max(|s_{j'}| - \tau, 0) \right] \vec{v}_j, \quad [6]$$

where s_j represents Pearson correlation coefficient between \vec{v}_j and \vec{c}_j , \vec{v}_j represents the respiratory signal from the j^{th} slice after the overall sign correction, and $\tau = 0.7$ is the correlation coefficient threshold. In Eq. 6, we sum over the weighted sign of correlations, with weights equal to $\max(|s_j| - \tau, 0)$, which effectively discard slices with low correlation. Then, the overall sign is based on the sign of this sum. Note, the quality of \vec{c}_j and thus the correlation of \vec{c}_j with \vec{v}_j can be poor for certain slices. As a result, this step by itself cannot be reliably used to adjust the sign for individual slices.

METHODS

MR acquisition

Our method was evaluated in vivo using data from eleven healthy volunteers and two patients. For the recruitment and consent of human subjects, the ethical approval was given by an Internal Review Board (2005H0124) at The Ohio State University. Two ten-slice short-axis stacks of RT cine covering the whole heart were acquired for each volunteer on a 1.5 T scanner (MAGNETOM Avanto, Siemens Healthcare, Erlangen, Germany), one under free-breathing and the other under end-expiration BH conditions, respectively. The BH acquisition was performed as a reference for cardiac function quantification. The acquisition time for each slice was 10 s to cover 1-3 respiratory cycles and 8-14 heartbeats. The slices were acquired sequentially with ECG trigger on. There was a small time gap (less than 1 s) between slices, and the starting respiratory phase for each slice was unknown and arbitrary. The other imaging parameters include: flip angle 69° , TE/TR 1.18/2.83 ms, pseudo-random Cartesian sampling with acceleration rate of 9 (25), slice thickness 8 mm, interslice gap 2 mm, FOV $\sim 300 \times 400$ mm, spatial resolution 1.6×1.6 mm², and temporal resolution 40–45 ms, resulting in 222–250 frames per slice. The two patients were scanned using the same protocol, with slightly worse temporal (~ 51 ms) and spacial ($\sim 2 \times 2$ mm²) resolutions on a 1.5 T scanner (MAGNETOM Sola, Siemens Healthcare, Erlangen, Germany) under free-breathing conditions. All the images were reconstructed inline using the Gadgetron (26) implementation of a parameter-free compressed sensing method called SCoRe (3).

Evaluation

As shown in Fig. 3, the respiratory motion extracted by non-rigid image registration (27) within a manually selected region-of-interest (ROI) was used as a reference. For each slice, the ROI was placed in an area with visibly pronounced respiratory motion. To capture the frame-to-frame respiratory motion, all frames for a given slice were registered to the first frame to produce 2D deformation fields with horizontal and vertical components. One of the components was averaged over the ROI to yield the reference signal across N frames. The appropriate component of the deformation field was selected based on the visual assessment of the motion within the ROI. For example, in Fig. 3(a), the ROI was selected on the chest wall, where the respiratory motion was predominantly along the anterior-posterior (AP) direction in the patient coordinate system. For this ROI, we chose the horizontal component of the deformation field since it aligns more closely with the AP direction. However, in Fig. 3(b), the ROI was selected on the liver dome, which moves along the SI direction. For this ROI, the vertical component of the deformation field was selected. To evaluate the agreement between the extracted respiratory signal, \vec{v}_j , and the reference, Pearson correlation coefficients were calculated for each slice. The directionality determination was considered to be correct when the correlation was positive.

As a comparison, we also implemented URE (17), where the lung-diaphragm interface is selected automatically using the eigen image of the middle slice of the short-axis stack; then, the directionality of the respiratory signal is determined by tracking the diaphragmatic motion or estimating the lung volume. Using multi-slice RT cine data from eleven volunteers and two patients, we compared our method to URE to extract the respiratory signal. For each method, all instances where the final respiratory signal had negative correlation with the reference were considered unsuccessful. Both methods were implemented Matlab (Mathworks, Natick, Massachusetts). The code of our method is provided on Github: <https://github.com/MRIOSU/AERC>.

Cardiac function quantification

Using the extracted respiratory signal as a guide, we selected one peak-expiration (PE) and one peak-inspiration (PI) heartbeat from each slice, and showed the respiratory motion-induced variations in cardiac output for healthy subjects. The quantification from the end-expiratory BH scan was chosen as the reference. For RT processing, arrhythmic heartbeats, defined as having a duration greater than fifteen percent different from the mean RR interval, were discarded from consideration.

Short-axis contours were initially generated automatically using the suiteHEART software (NeoSoft LLC, Pewaukee, WI) and then were visually assessed frame-by-frame and modified manually when necessary. In this study, trabeculations and papillary muscles were considered part of the right and left ventricular blood pools. After the summation of all slices, suiteHEART calculated the end-diastolic volume (EDV) and end-systolic volume (ESV) automatically for each ventricle. The analysis was firstly performed in volunteers for the PE heartbeats, and then repeated for the PI heartbeats using the same protocol.

RESULTS

Performance in healthy volunteers

Fig. 4(a) shows the absolute values of Pearson correlation coefficients $|r_{j,j+1}|$ between neighboring eigen images, $\mathbf{D}_j\vec{v}_j$ and $\mathbf{D}_{j+1}\vec{v}_{j+1}$, for all the volunteers. The mean and standard deviation of $|r_{j,j+1}|$ is 0.65 ± 0.16 . Fig. 4 (b) shows the Pearson correlation coefficients, s_j , between \vec{v}_j and ZMC curve, \vec{c}_j . As highlighted by the red arrows, the sign of s_j is incorrect for some individual slices due to the poor quality of the ZMC curve. Therefore, the ZMC curve itself cannot be used to determine the sign for individual slices. However, the overall sign correction using Eq. 6 is robust because it is based on consensus from all slices that exhibit strong correlation between \vec{c}_j and \vec{v}_j .

Pearson correlation coefficients between the extracted respiratory motion and the reference for healthy subjects are summarized in Table 1. We report the mean, standard derivation (SD), median, and range across 10 slices for each subject. In all cases, the extracted respiratory signal exhibit high, positive correlation with the reference. Fig. 5 shows results from two representative volunteers, one with short respiratory cycles and the other with long cycles. The proposed method works well across different respiratory patterns. As highlighted by the red arrow, this method is also tolerant of irregular respiratory motion. For some slices in Fig. 5, the discrepancy between the proposed method and reference is more pronounced. This is not surprising because the two methods measure different quantities: the reference (non-rigid image registration) extracts the respiratory motion from a user-defined ROI, while the proposed PCA-based method tracks the motion from the entire image.

Fig. 6 shows the respiratory signals extracted using our method, URE, and the non-rigid registration reference for two volunteers. URE determined the directionality of the respiratory signal

correctly for all the other volunteers but failed in two slices shown here. One of the failures was caused by the wrong selection of lung-diaphragm interface, and the other by the incorrect directionality of the signal estimated from the lung volume. In contrast, our method corrected the directionality of the respiratory signal successfully for all the cases. We also observed that there are more cardiac motion-induced oscillations in the non-rigid registration reference in Fig. 6; it is expected because no filter is applied during the extraction of the reference signal. The averaged processing time (Intel Core i5, 2.7 GHz, 16 GB) for one volunteer using our method and URE was 10.0 s and 13.4 s, respectively.

Heartbeat selection and cardiac function quantification

Fig. 7 shows the PE and PI heartbeats selected using the extracted respiratory signal as a guide for one volunteer. In the end-diastolic frames, all slices within PE have elevated liver dome compared to the corresponding PI slices. Significant in-plane and through-plane motion of the heart can be noticed between PE and PI heartbeats, highlighting the perils of performing quantification from slices with disparate respiratory phases. Fig. 8 summarizes the results of cardiac function quantification for both ventricles. EDV, ESV, their mean and standard deviation across ten volunteers are reported here. For one volunteer, there was visible misalignment between the BH and free-breathing scans, potentially due to the patient motion; this subject was excluded from cardiac function quantification. For each of the remaining ten volunteers, quantification results from BH, PE, and PI are reported, with BH serving as reference. PE and PI represent quantification performed from peak-expiration and peak-inspiration heartbeats. As shown in Fig. 8(a), for the right ventricle, there is a significant increase ($p < 0.01$) from PE to PI both in EDV and ESV, and the quantification of PE is in agreement with reference BH. These findings are consistent with the literature (6). However, for the left ventricle, the differences between BH, PE, and PI are not significant, which is likely due to the sample size being inadequate to distinguish smaller variations in left ventricle (LV) function (6, 28).

Performance in patients

Fig. 6 demonstrates the respiratory signals extracted using our method, URE and the non-rigid registration reference for the two patients. All the methods performed reasonably well in the second patient, who had a periodic respiratory pattern. However, for the first patient with irregular breath-

ing motion, the respiratory signal extracted using the proposed method is in better agreement with the non-rigid registration reference.

DISCUSSION

To accurately and reproducibly measure LV and right ventricle (RV) cardiac function, it is essential to determine the respiratory phase of the images. The feasibility of dimensionality reduction-based methods to extract the respiratory signal has been previously demonstrated. However, none of these methods preserve the directionality of respiratory signal, and therefore cannot reliably distinguish between inspiratory and expiratory motion, which can lead to inaccurate cardiac function quantification. We propose and evaluate a new method to correctly assign the directionality (sign) of the respiratory signal where no ROI and tuning parameters are induced. The method utilizes the similarity of neighboring eigen images to adjust the sign of all slices with respect to the first slice. Then, the zeroth-moment center, ZMC, is used to adjust the global sign. In this work, linear PCA is used to extract the respiratory signal; however, the proposed directionality determination procedure can be incorporated with other dimensionality reduction-based methods for respiratory signal extraction.

In the volunteer study, we evaluated our method in 11 subjects. The respiratory signal extracted using non-rigid image registration from a manually selected ROI is chosen as the reference. To evaluate the reliability of our method, we have shown the absolute values of Pearson correlation coefficients $|r_{j,j+1}|$ between neighboring eigen images and the Pearson correlation coefficients, s_j , between \vec{v}_j and the ZMC curve \vec{c}_j in Fig. 4. The content of neighboring slices is expected to be similar but not identical; hence, the values of $|r_{j,j+1}|$ are significantly less than one. However, our preliminary findings show that these values are sufficiently reliable to adjust the sign of all slices with respect to the reference slice. After the first step of our directionality (sign) determination procedure, the sign of \vec{v}_j is consistent for all values of j . If the ZMC curve is accurate, s_j should have the same sign, either positive or negative, for all j . However, as highlighted by the red arrows in Fig.4(b), the sign of s_j is incorrect for certain slices due to the poor quality of \vec{c}_j , which means the ZMC curve by itself cannot be used to determine the sign for individual slices. As shown in Fig. 5, the proposed method is robust across different respiratory patterns, even for irregular respiratory motion. Since the reference only tracks the motion in the selected ROI, while the proposed method extracts the respiratory motion from the entire image, the difference between them is pronounced for

some slices. Overall, our method determined the directionality of the respiratory signal successfully in all cases.

Although linear PCA was used to extract the respiratory signal from RT cardiac cine MRI both in this work and in URE (17), there are minor differences between the two approaches: (i) In our method, the images are pre-filtered to suppress the cardiac motion and (ii) the temporal mean is subtracted before applying the linear PCA. Consequently, our largest singular vector consistently captures the respiratory motion. In contrast, the first singular vector in URE is the DC component and the second singular vector is the respiratory signal, which is then filtered using a Savitzky–Golay filter to remove cardiac signal. With the cardiac motion filtered and the temporal mean subtracted before PCA, our method is more robust in localizing the respiratory motion to the first singular vector. Without these two additional processing steps, it is feasible that the temporal mean, respiratory motion, and cardiac motion are not localized in the first, second and third singular vectors, respectively, leading to contamination of the extracted respiratory signal. Our directionality determination procedure, which is the major contribution of this work, is distinct from URE. URE determined the directionality of the respiratory signal by tracking the diaphragmatic motion or estimating the lung volume, where the lung-diaphragm interface is automatically identified. However, in this work, we propose a two-step procedure to perform the directionality determination, where no ROI and tuning parameters are induced.

To demonstrate the clinical utility of our method, we selected PE and PI heartbeats from each slice using the extracted respiratory signal as a guide. As shown in Fig. 7, both significant in-plane and through-plane motion can be noticed between the PE and PI heartbeats. Several studies have investigated the influence of breathing in left and right ventricular volumes. During normal breathing, inspiration results in a significant increase in RV volumes and a small decrease in LV volumes. In this work, we observed a significant increase ($p < 0.001$) from PE to PI both for RV EDV and RV ESV, which is consistent with the the physiology (6) and highlight the potential adverse affect of mixing slices from different respiratory phases. However, for the LV volume, we did not observe a significant difference between the PE and PI heartbeats. This could be because the small sample size is inadequate to distinguish variations in LV function, which is less susceptible to respiratory-induced motion (28). We also compared the two methods using data from two patients, one with a periodic respiratory pattern and the other with an irregular respiratory pattern. As shown in Fig. 9, both methods performed well when the respiratory pattern was periodic; however, for the patient with irregular breathing motion, our method exhibited better agreement with the

reference.

We recognize that the proposed method has several limitations. One of them is the expectation that the respiratory signal is confined to the first singular vector. Besides the eleven subjects included in this study, we collected data from one more volunteer. Due to the significant bulk motion during the scan, this volunteer was excluded from the study. Nonetheless, we observed that the first singular vector, for this specific volunteer, captured the bulk motion instead of the respiratory motion. As it has been reported previously (17), the presence of another motion source, can threaten the localization of the respiratory motion to one singular vector. Another limitation of this study is the lack of validation for the cases with shorter scan time (< 10 s). In this work, all the subjects were scanned for 10s per slice to cover 1-3 respiratory cycles. Since both the low pass filter and PCA benefit from the long scan, we expect that both the performance of our method and URE to degrade for shorter scans. In order to explore the influence of shorter scan time, we separated each 10s cine series into two 5s series. We found that the directionality in 1 and 3 cases were incorrectly determined for 5s series using the proposed method and URE, respectively. Since the proposed method utilizes the correlation of neighboring eigen images (Eq. 3), the incorrect directionality assignment for the l^{th} slice may transmit to the following slices ($j > l$). We did not encounter this problem in the 10s and 5s series, but this is a potential risk for shorter scan times. To accommodate this potential limitation, non-rigid registration could be applied on neighboring eigen images to increase their correlation from a shorter scan. Finally, this study does not include a large number of subjects with inconsistent breathing.

CONCLUSION

We have proposed a fully automatic method to extract the respiratory signal and to correctly identify the directionality of the respiratory phase in each slice. Linear PCA is applied to the preprocessed temporal image series to extract the respiratory motion. Then a two-step procedure is used to determine the directionality (sign) of the respiratory signal: (i) utilize the similarity of neighboring eigen images to adjust the sign of all slices with respect to the first slice; (ii) use the ZMC curve to perform the global sign correction. The proposed method was used to extract and determine the directionality of the respiratory signal successfully for 11 volunteers and 2 patients. Using the extracted respiratory signal as a guide, we selected one PE and PI heartbeats from each slice and demonstrated the respiratory motion induced variations in cardiac output in volunteers.

The proposed method requires no user-defined ROI or tuning parameters and was shown to be more reliable than another recently described method.

ACKNOWLEDGMENTS

This work was funded in part by NIH project R01HL135489.

References

- [1] Feng L, Srichai MB, Lim RP, Harrison A, King W, Adluru G, et al. Highly accelerated real-time cardiac cine MRI using k-t SPARSE-SENSE. *Magnetic Resonance in Medicine* 2013;70(1):64–74.
- [2] Kellman P, Chefd’hotel C, Lorenz CH, Mancini C, Arai AE, McVeigh ER. High spatial and temporal resolution cardiac cine MRI from retrospective reconstruction of data acquired in real time using motion correction and resorting. *Magnetic Resonance in Medicine* 2009;62(6):1557–1564.
- [3] Chen C, Liu Y, Schniter P, Jin N, Craft J, Simonetti O, et al. Sparsity adaptive reconstruction for highly accelerated cardiac MRI. *Magnetic Resonance in Medicine* 2019;81(6):3875–3887.
- [4] Wu Y, Jiang K, Zhang N, Gao Y, Chen Y, Zheng H, et al. Efficient method for analyzing MR real-time cines: Toward accurate quantification of left ventricular function. *Journal of Magnetic Resonance Imaging* 2015;42(4):972–980.
- [5] Wu Y, Wan Q, Zhao J, Liu X, Zheng H, Chung YC, et al. Improved workflow for quantifying left ventricular function via cardiorespiratory-resolved analysis of free-breathing MR real-time cines. *Journal of Magnetic Resonance Imaging* 2017;46(3):905–914.
- [6] Claessen G, Claus P, Delcroix M, Bogaert J, Gerche AL, Heidbuchel H. Interaction between respiration and right versus left ventricular volumes at rest and during exercise: a real-time cardiac magnetic resonance study. *American Journal of Physiology-Heart and Circulatory Physiology* 2014;306(6):H816–H824.
- [7] Wang Y, Rossman PJ, Grimm RC, Riederer SJ, Ehman RL. Navigator-echo-based real-time

- respiratory gating and triggering for reduction of respiration effects in three-dimensional coronary MR angiography. *Radiology* 1996;198(1):55–60.
- [8] Santelli C, Nezafat R, Goddu B, Manning WJ, Smink J, Kozerke S, et al. Respiratory bellows revisited for motion compensation: preliminary experience for cardiovascular MR. *Magnetic Resonance in Medicine* 2011;65(4):1097–1102.
- [9] Larson AC, White RD, Laub G, McVeigh ER, Li D, Simonetti OP. Self-gated cardiac cine MRI. *Magnetic Resonance in Medicine* 2004;51(1):93–102.
- [10] Crowe ME, Larson AC, Zhang Q, Carr J, White RD, Li D, et al. Automated rectilinear self-gated cardiac cine imaging. *Magnetic Resonance in Medicine* 2004;52(4):782–788.
- [11] Bögel M, Hofmann HG, Hornegger J, Fahrig R, Britzen S, Maier A. Respiratory motion compensation using diaphragm tracking for cone-beam C-arm CT: A simulation and a phantom study. *International Journal of Biomedical Imaging* 2013;2013.
- [12] Tran EH, Eiben B, Wetscherek A, Oelfke U, Meedt G, Hawkes DJ, et al. Evaluation of MRI-derived surrogate signals to model respiratory motion. *Biomedical Physics & Engineering Express* 2020;.
- [13] Bundschuh RA, Martínez-Moeller A, Essler M, Martínez MJ, Nekolla SG, Ziegler SI, et al. Postacquisition detection of tumor motion in the lung and upper abdomen using list-mode PET data: a feasibility study. *Journal of Nuclear Medicine* 2007;48(5):758–763.
- [14] Kellman P, Chefd’hotel C, Lorenz CH, Mancini C, Arai AE, McVeigh ER. Fully automatic, retrospective enhancement of real-time acquired cardiac cine MR images using image-based navigators and respiratory motion-corrected averaging. *Magnetic Resonance in Medicine* 2008;59(4):771–778.
- [15] Thielemans K, Rathore S, Engbrant F, Razifar P. Device-less gating for PET/CT using PCA. In: 2011 IEEE Nuclear Science Symposium Conference Record IEEE; 2011. p. 3904–3910.
- [16] Ma H, Dibildox G, Schultz C, Regar E, van Walsum T. PCA-derived respiratory motion surrogates from X-ray angiograms for percutaneous coronary interventions. *International Journal of Computer Assisted Radiology and Surgery* 2015;10(6):695–705.

- [17] Novillo F, Van Eyndhoven S, Moeyersons J, Bogaert J, Claessen G, La Gerche A, et al. Un-supervised respiratory signal extraction from ungated cardiac magnetic resonance imaging at rest and during exercise. *Physics in Medicine & Biology* 2019;64(6):065001.
- [18] Fischer P, Pohl T, Faranesh A, Maier A, Hornegger J. Unsupervised learning for robust respiratory signal estimation from X-Ray fluoroscopy. *IEEE Transactions on Medical Imaging* 2016;36(4):865–877.
- [19] Thielemans K, Schleyer P, Marsden PK, Manjeshwar RM, Wollenweber SD, Ganin A. Comparison of different methods for data-driven respiratory gating of PET data. In: 2013 IEEE Nuclear Science Symposium and Medical Imaging Conference (2013 NSS/MIC) IEEE; 2013. p. 1–4.
- [20] Sanders JC, Ritt P, Kuwert T, Vija AH, Maier AK. Fully automated data-driven respiratory signal extraction from SPECT images using Laplacian eigenmaps. *IEEE Transactions on Medical Imaging* 2016;35(11):2425–2435.
- [21] Usman M, Atkinson D, Kolbitsch C, Schaeffter T, Prieto C. Manifold learning based ECG-free free-breathing cardiac CINE MRI. *Journal of Magnetic Resonance Imaging* 2015;41(6):1521–1527.
- [22] Bertolli O, Arridge S, Wollenweber SD, Stearns CW, Hutton BF, Thielemans K. Sign determination methods for the respiratory signal in data-driven PET gating. *Physics in Medicine & Biology* 2017;62(8):3204.
- [23] Chen C, Liu Y, Simonetti OP, Ahmad R. Automatic Extraction and Sign Determination of Respiratory Signal in Real-Time Cardiac Magnetic Resonance Imaging. In: 2020 IEEE 17th International Symposium on Biomedical Imaging (ISBI) IEEE; 2020. p. 1–4.
- [24] Wang Y, Riederer SJ, Ehman RL. Respiratory motion of the heart: kinematics and the implications for the spatial resolution in coronary imaging. *Magnetic Resonance in Medicine* 1995;33(5):713–719.
- [25] Ahmad R, Xue H, Giri S, Ding Y, Craft J, Simonetti OP. Variable density incoherent spatiotemporal acquisition (VISTA) for highly accelerated cardiac MRI. *Magnetic Resonance in Medicine* 2015;74(5):1266–1278.

- [26] Hansen MS, Sørensen TS. Gadgetron: an open source framework for medical image reconstruction. *Magnetic Resonance in Medicine* 2013;69(6):1768–1776.
- [27] Chéfd'Hotel C, Hermosillo G, Faugeras O. Flows of diffeomorphisms for multimodal image registration. In: *Proceedings IEEE International Symposium on Biomedical Imaging IEEE*; 2002. p. 753–756.
- [28] Liu J, Wang Y, Wen Z, Feng L, Lima APS, Mahadevan VS, et al. Extending cardiac functional Assessment with Respiratory-Resolved 3D Cine MRI. *Scientific Reports* 2019;9(1):1–10.

Pearson correlation coefficient			
Volunteer	Mean±SD	Median	Range
1	0.95±0.02	0.96	0.90–0.97
2	0.91±0.03	0.91	0.87–0.95
3	0.94±0.04	0.95	0.87–0.97
4	0.93±0.10	0.96	0.66–0.99
5	0.92±0.05	0.93	0.81–0.98
6	0.93±0.04	0.95	0.86–0.97
7	0.92±0.04	0.93	0.86–0.98
8	0.93±0.05	0.95	0.82–0.99
9	0.92±0.08	0.94	0.73–0.98
10	0.96±0.03	0.98	0.90–0.99
11	0.97±0.03	0.98	0.88–0.99

Table 1: Pearson correlation coefficients between the extracted respiratory motion and the reference. Ten slices were scanned for each volunteer and the correlation coefficient was calculated slice-wise.

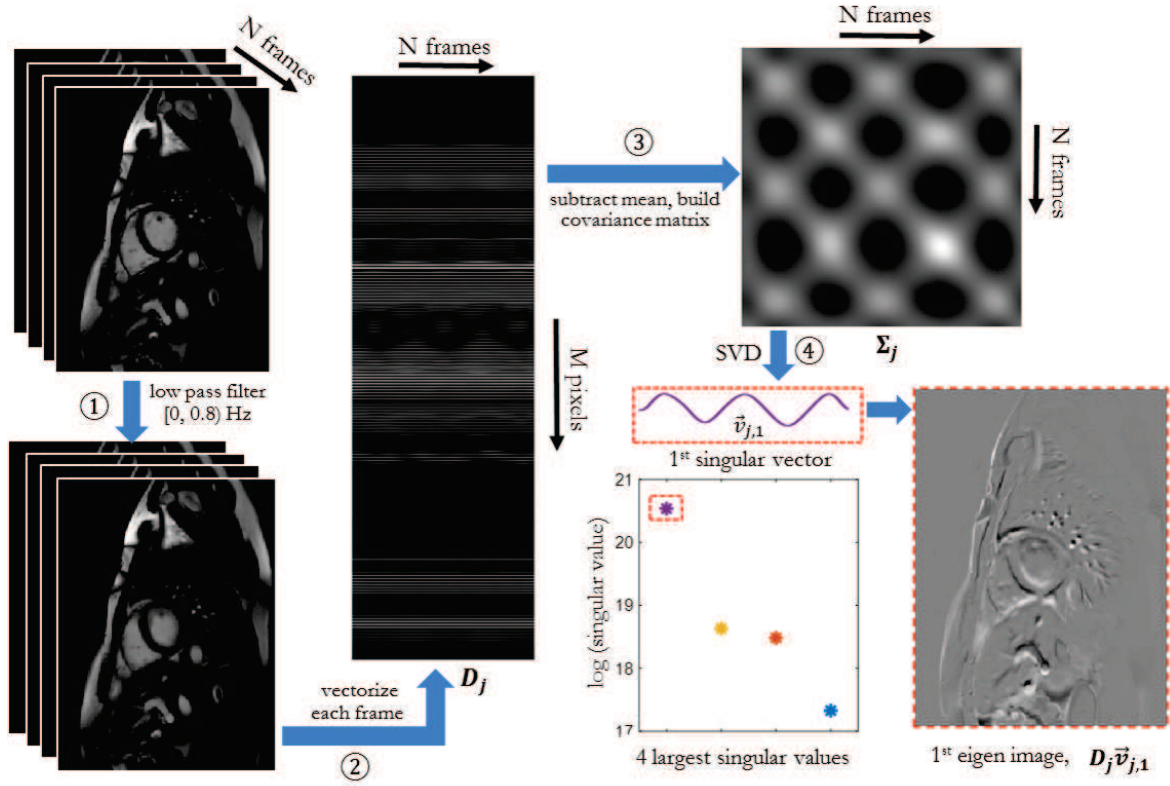
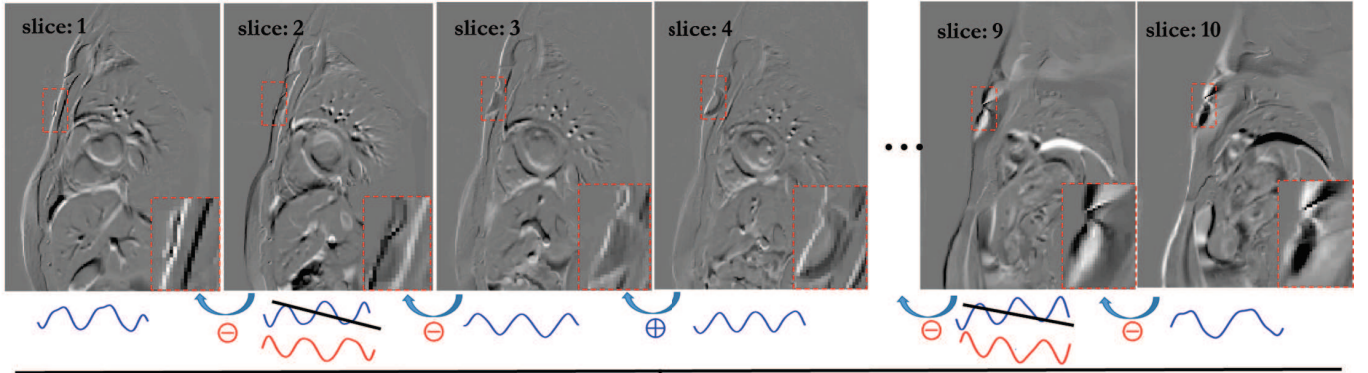
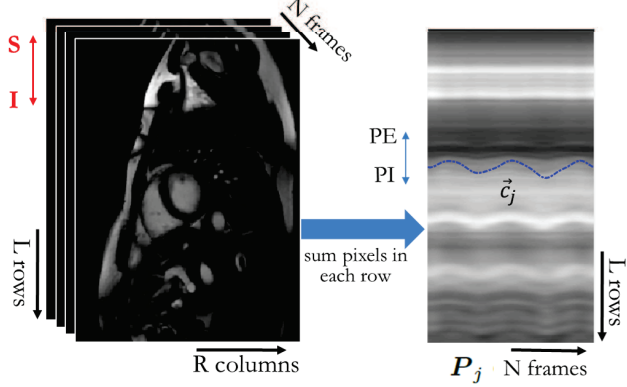


Figure 1: Extraction of the respiratory signal from the j^{th} slice. First, a low-pass filter $[0 - 0.8 \text{ Hz}]$ is applied along the temporal dimension to suppress the cardiac motion. Second, the image series is flattened into a matrix, D_j . Third, temporal mean is subtracted from D_j (Eq. 1), and the resulting matrix is used to compute the covariance matrix, Σ_j (Eq. 2). Fourth, eigen decomposition is performed, with the first singular vector, $\vec{v}_{j,1}$, corresponding to the respiratory signal. Finally, the 1st “eigen image” is obtained by $D_j \vec{v}_{j,1}$, which can be interpreted as a projection of the image series on the corresponding respiratory signal and is used in the directionality determination procedure.

(a) adjust the sign of all slices respect to the reference (1st slice)

 (b) extract ZMC curve \vec{c}_j


(c) overall sign correction

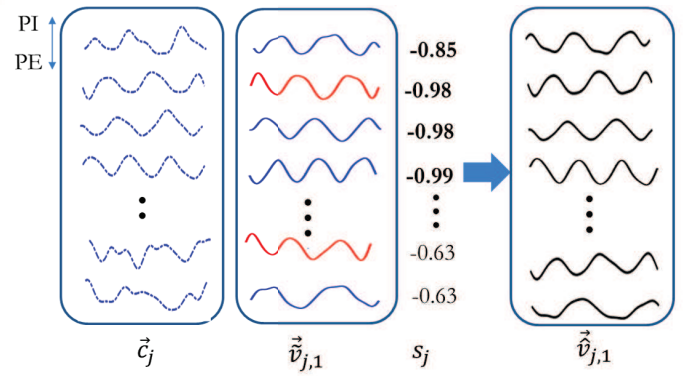


Figure 2: Proposed directionality (sign) determination procedure. (a) Step 1: A pair-wise inter-slice correlations are used to fix the sign of individual slices with respect to the reference (1st slice). (b,c) Step 2: An overall sign correction is performed using the correlations, s_j , of slices with \vec{c}_j . Here, S and I represent superior and inferior directions, respectively, and PE and PI represent peak-expiration and peak-inspiration, respectively.

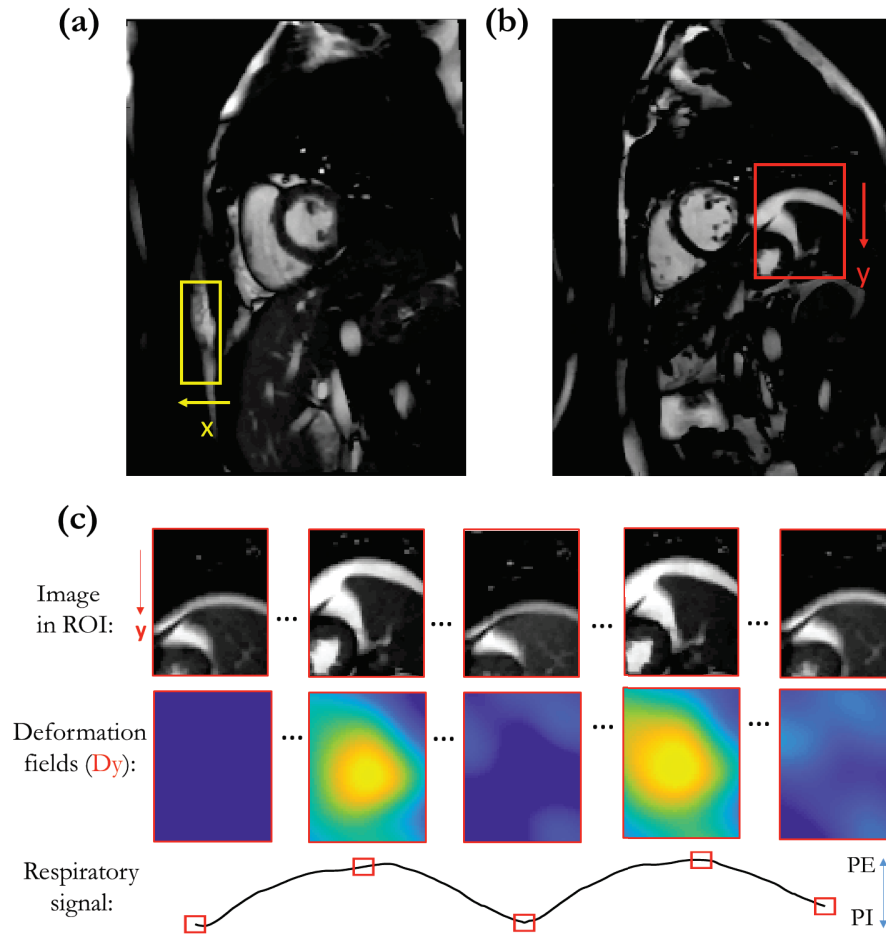


Figure 3: (a, b) Manually placed ROI (red and yellow boxes) for two different volunteers. (c) The pipeline to extract the respiratory motion using non-rigid image registration. Five different frames are shown for the image in (b), along with the y -component of the deformation field, D_y . The spatial average of D_y yields the respiratory signal.

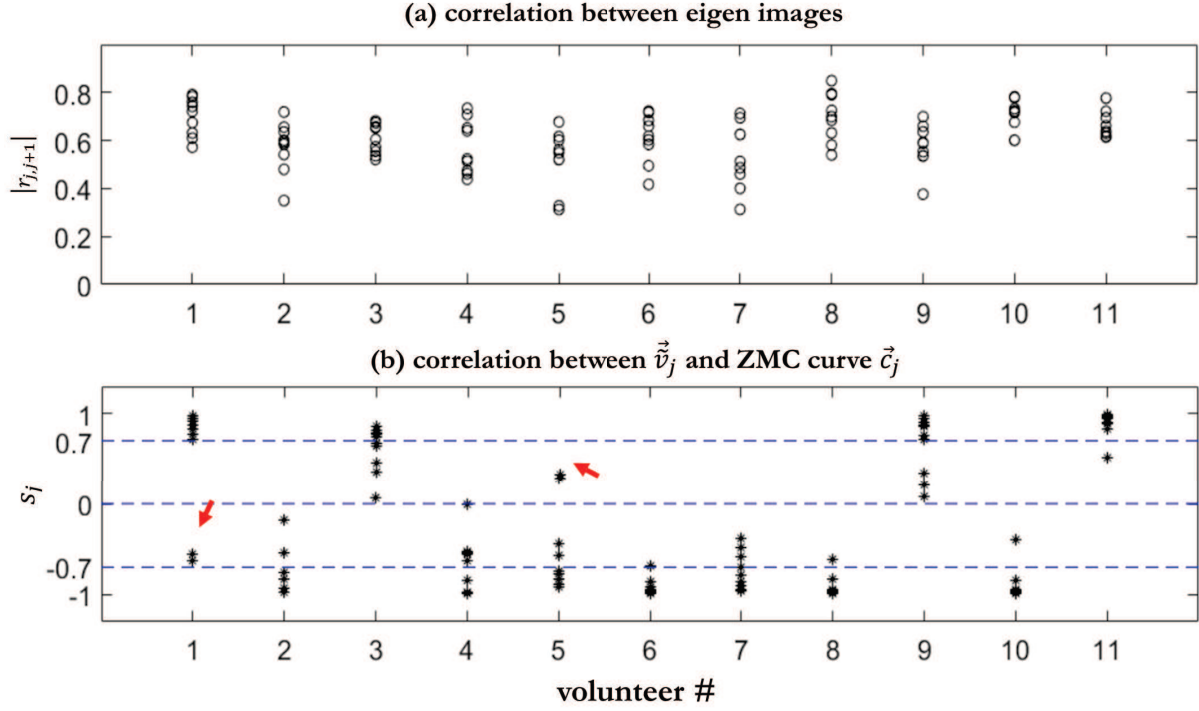


Figure 4: (a) The absolute values of Pearson correlation coefficients $|r_{j,j+1}|$ between eigen-images, i.e., $D_j \vec{v}_j$ and $D_{j+1} \vec{v}_{j+1}$, which are used in the first step of our directionality determination procedure. (b) Pearson correlation coefficients s_j between \vec{v}_j and ZMC curve \vec{c}_j used for overall sign correction in the second step. The red arrows highlight instances where the signs of individual slices are incorrect.

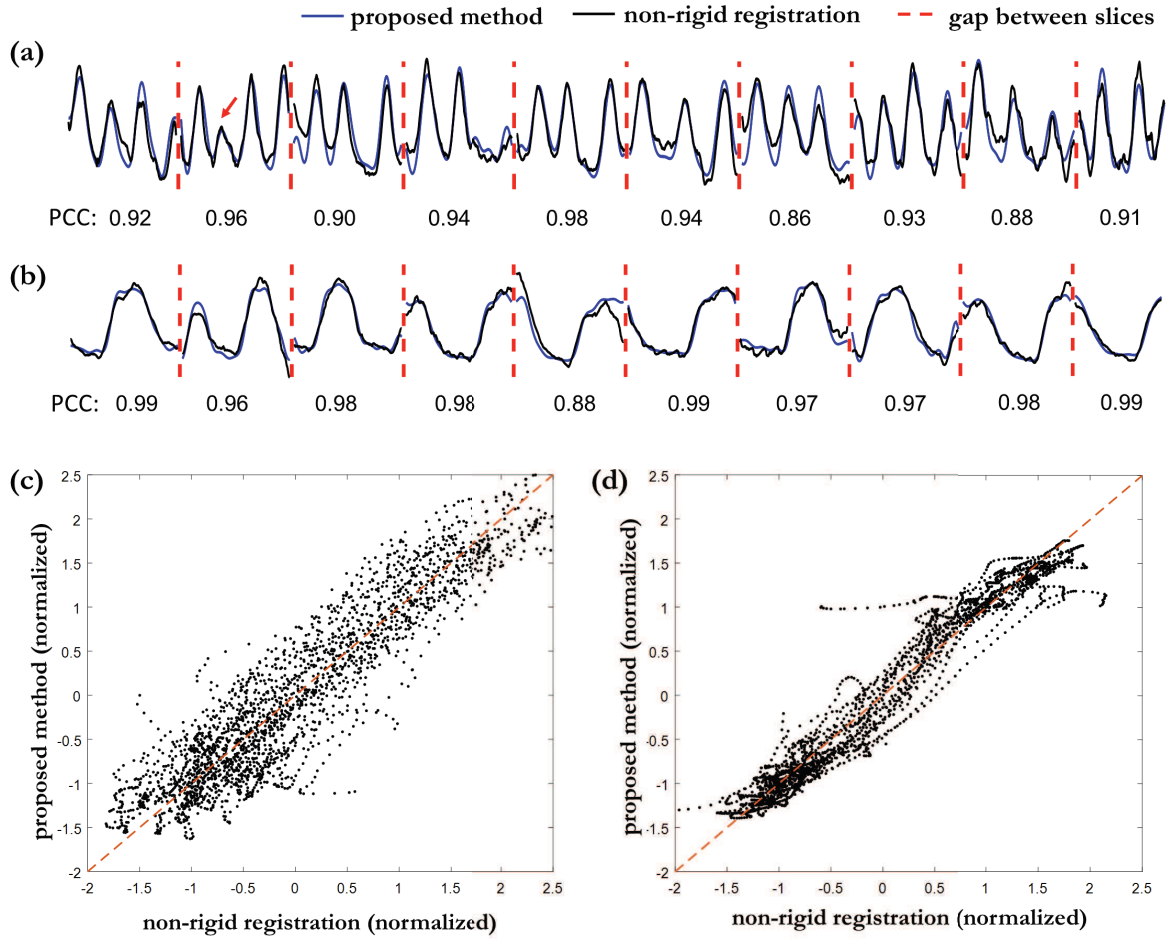


Figure 5: (a, b) The respiratory signal from the proposed method and the reference superimposed. (c, d) Scatter plots between the extracted and reference respiratory signals in (a) and (b). The results from two representative volunteers are shown, one with short respiratory cycles (a, c) and the other with long cycles (b, d). The red arrow highlighting the irregular respiratory motion. PCC is the Pearson correlation coefficient between signals from the proposed method and the reference.

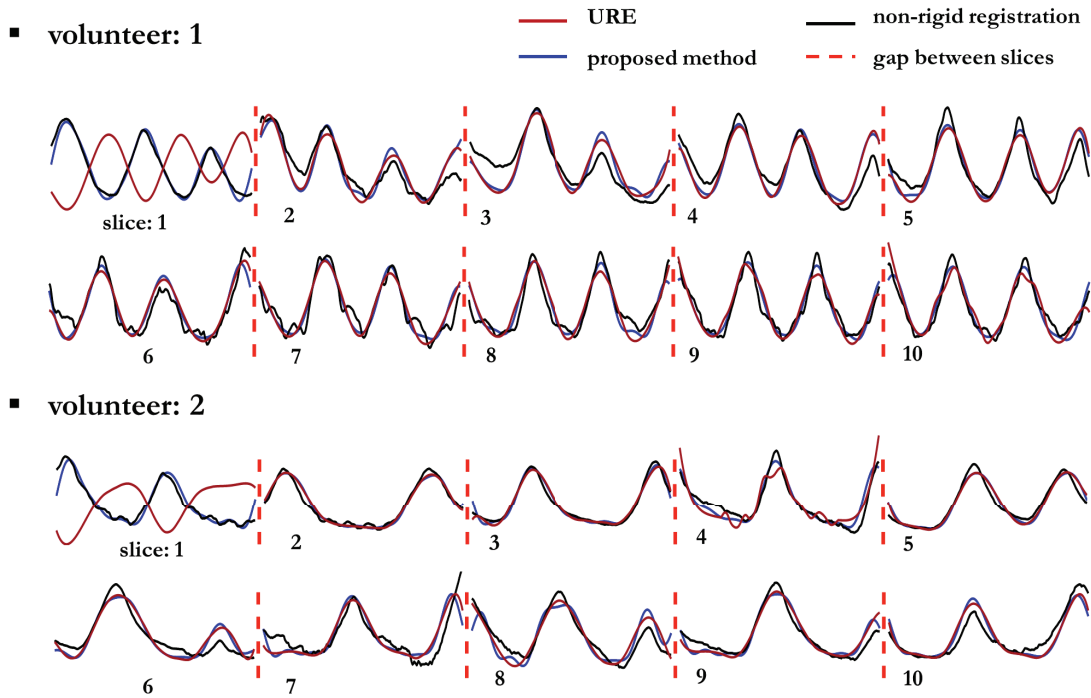


Figure 6: A direct comparison of the respiratory signals extracted using the proposed method and the method by Novillo et al. (URE). The results are shown for two volunteers. URE determined the directionality of the respiratory signal correctly for all the other volunteers, but failed in the two slices shown here.

PE vs. PI heartbeats (end diastolic frames)

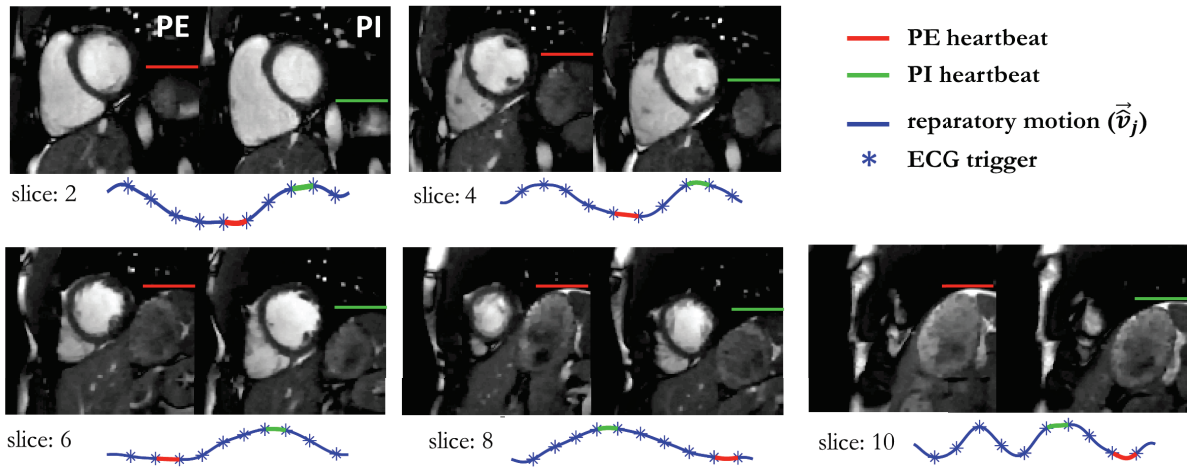
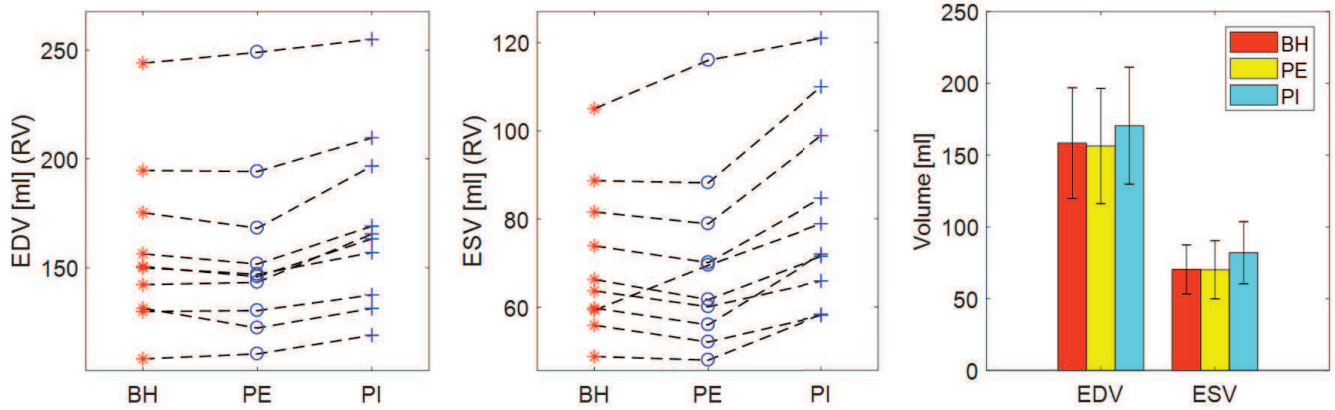


Figure 7: Peak expiration (PE) and peak inspiration (PI) heartbeats identified using the proposed method. Images from five different slices are shown. The position of the liver dome is tracked with red (PE) and green (PI) lines. As expected, the position of the liver dome is lower in PI than in PE. The through plane motion between PE and PI is also obvious from the size of the RV. Only an end-diastolic frame is shown for one volunteer.

(a) cardiac function quantification for right ventricle (RV)



(b) cardiac function quantification for left ventricle (LV)

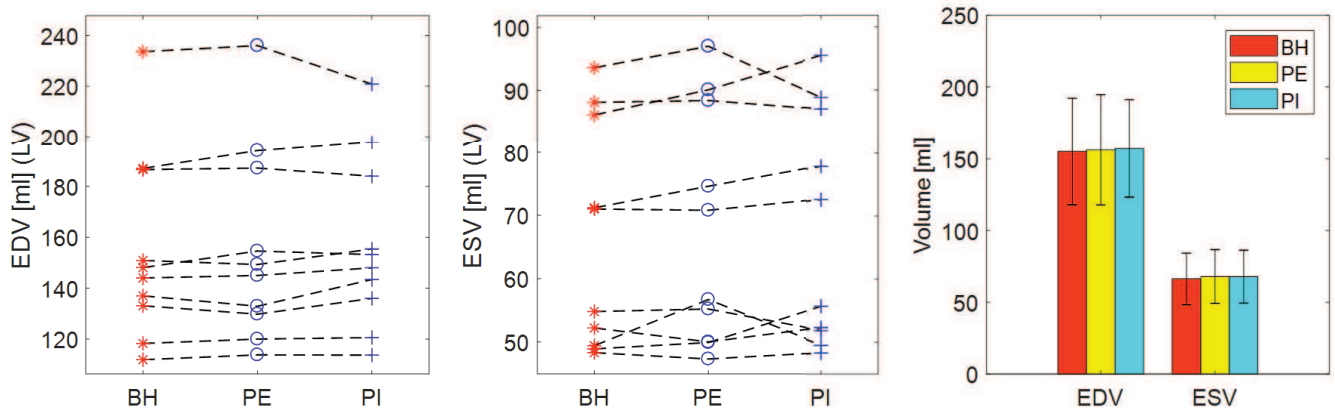


Figure 8: Cardiac function quantification for the right (a) and left (b) ventricle. EDV and ESV are reported here. Each line in the figure represents the result from a single volunteer. The bar chart shows the mean and standard deviation of EDV and ESV across all the volunteers.

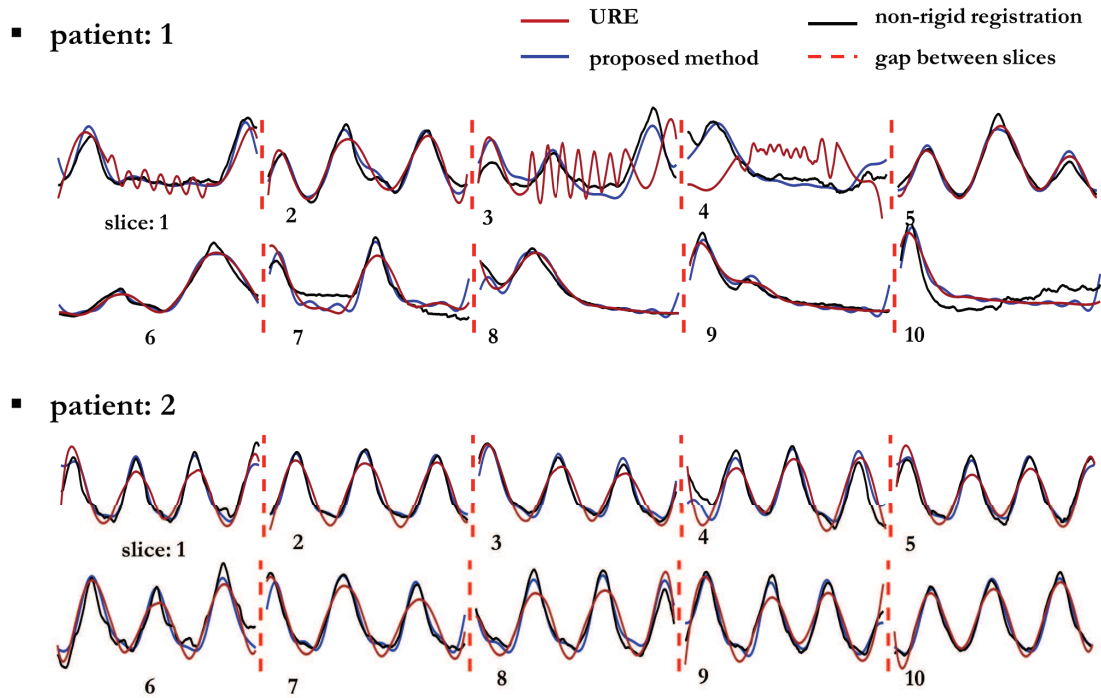


Figure 9: A direct comparison of the respiratory signals extracted using the proposed method and the method by Novillo et al. (URE). The results are shown for two patients.